

# High-Fidelity Computational Methodology for Stitched Composite Aerospace Structures

Brandon Horton<sup>1</sup>, Yangkun Song<sup>1</sup>, Dawn Jegley<sup>2</sup>, and Javid Bayandor<sup>3</sup>

## ABSTRACT

Due to the high demands for energy efficient commercial transportation, the aviation industry has taken a leading role in the integration of composite structures. Among the leading concepts to develop lighter, more fuel-efficient commercial transport is the Pultruded Rod Stitched Efficient Unitized Structure (PRSEUS) concept, an enabling technology for hybrid wing bodies. Many proof-of-concept tests have been performed to demonstrate that the use of PRSEUS has improved the residual strength of damaged structures compared to conventional composite structures, but efficient computational tools must be developed before the concept can be commercially certified and implemented. In an attempt to address the need for efficient computational tools, a comprehensive modeling approach is developed and applied to investigate applications of PRSEUS at multiple scales. Therefore, a computational methodology has been progressively developed based on physically realistic concepts. The focus of the work described herein is to define the modeling characteristics required to accurately simulate the damage progression and failure of PRSEUS at the coupon scale. The work herein is focused on the development and analysis of a PRSEUS stringer, the methodology for which may be extended to other PRSEUS coupons and components.

## INTRODUCTION

The hybrid wing body (HWB), also known as the blended wing body (BWB), is one of the leading innovative concepts to replace the conventional tube-wing aircraft design [1]. The modern interpretation of the wing-body structure was initially discussed by Liebeck in 1988 [2]. Later in 1994, a team of researchers with multidisciplinary backgrounds investigated the HWB concept to initiate a revolution in aircraft design and development [3]. The unique contouring of the aircraft body provides many advantages compared to typical aircraft today. In conventional tube-wing aircraft, lift is produced primarily by the wing. Alternatively, the HWB concept utilizes the unique design of its fuselage to create lift across the entire body. The reduced drag and increased lift production of the fuselage can reduce fuel consumption, while also increasing the payload capacity by allowing storage over a much greater surface area [4]. Due to these potential advantages, the HWB concept has been investigated by many different disciplines [5–9] in order to realize this revolutionary concept in high-efficiency subsonic transport. While the HWB may one day replace

---

<sup>1</sup> Research Engineer at *CR*ashworthiness for Aerospace Structures and *H*ybrids (*CRASH*) Lab, Department of Mechanical and Aerospace Engineering, University at Buffalo

<sup>2</sup> Senior Research Aerospace Engineer, NASA Langley Research Center

<sup>3</sup> Founder and Director of *CRASH* Lab, Department of Mechanical and Aerospace Engineering, University at Buffalo

the current commercial aircraft design, the unique fuselage geometry introduces many additional complexities.

One of the primary concerns from the structural perspective is the complex pressure distribution developed on the interior of a HWB. For conventional tube-wing fuselage design, the stress caused by the internal pressure is easily evaluated by using well-established hoop stress calculations. The hoop stress is directly proportional to the internal pressure and radius of the tubular structure, and inversely to the skin thickness. In a HWB, however, this hoop stress calculation is no longer valid due to the almost-flat surfaces and right-angle corners in the center cabin section. Due to this unique geometry, physical experiments have been conducted to test the structural integrity as a function of the pressure load for new structural technologies designed for the HWB [10]. In addition to the complex internal pressure distribution, the flight loads present on the wing are directly transferred to the cabin section of the HWB as shown in Fig. 1. Therefore, the structure of a HWB requires a new structural concept to be developed in order to sustain the combination of out-of-plane and aerodynamic loads on the aircraft without adding excessive weight to the structure.

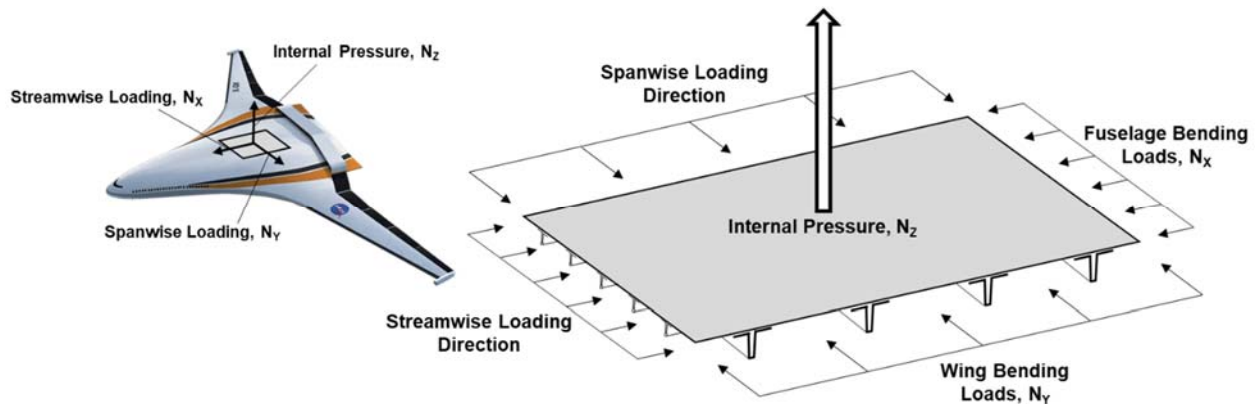


Figure 1. Schematic of loads present in a pressurized, non-tubular fuselage such as the HWB

One such structural concept is the Pultruded Rod Stitched Efficient Unitized Structure (PRSEUS), developed by a collaboration between NASA and The Boeing Company (Boeing) and shown in Fig. 2. Carbon fiber-reinforced polymer (CFRP) composites are well-known for their outstanding strength-to-weight ratio relative to aerospace grade metal alloys. For the material configuration analyzed in the current research, seven layers of CFRP are arranged in a “stack” of material in a  $[+45/-45/0/90/0/-45/+45]$  sequence with a (44/44/12) fiber architecture, where the values are percentages of (0/ $\pm 45/90$ ) degree plies. Each stack has a total thickness of 1.321 mm (0.052 inches). Thicker sections are built by layering stacks. The PRSEUS concept uses a carbon fiber pultruded rod in conjunction with unidirectional CFRP laminates that are stitched together to overcome the most prominent problem in composite failure, delamination. Among other significant improvements, the ability of PRSEUS to arrest delamination propagation gives PRSEUS a huge advantage over conventional composites. During manufacturing, threads are stitched through skin, tear strap, and flange stacks and bind the PRSEUS components into a single part. Then, this part is co-cured using the state-of-the-art Controlled Atmosphere Pressure Resin Infusion (CAPRI) process [11], producing a high-strength bond. Unlike metallic structures, this

advanced stitched composite structure does not require rivets or other external connections, reducing the weight of the airframe significantly. A more in-depth summary of the PRSEUS concept and fabrication process can be found in [12, 13].

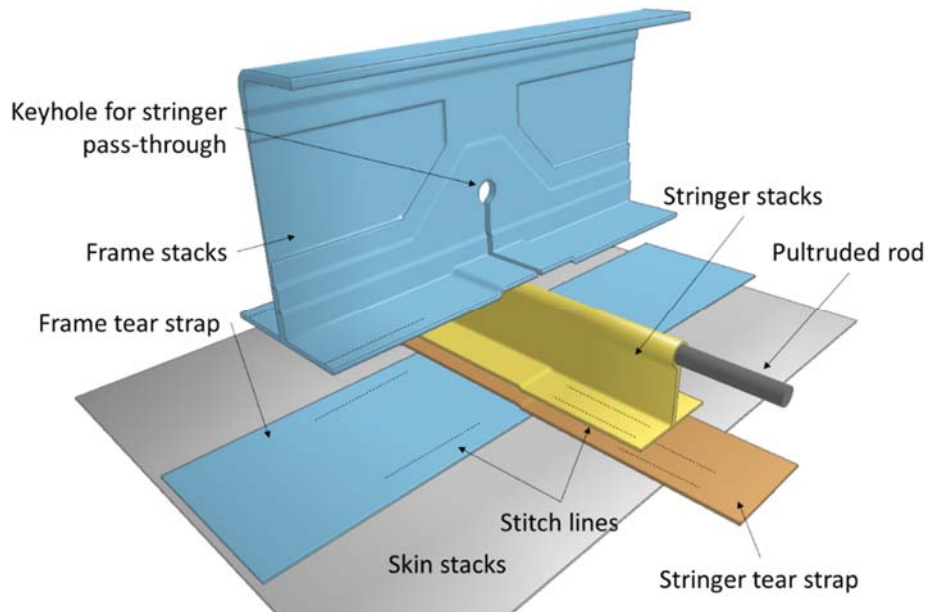


Figure 2. Exploded view of the PRSEUS concept

The majority of the existing research on PRSEUS has focused on experimental characterization, with some complementary computational analysis to capture non-local, global response [14–16]. For the sake of computation time, the numerical models used in the majority of the preceding studies are relatively low-fidelity or exclude critical damage mechanics, which reduce the accuracy of the predictions and can prevent a realistic estimate of buckling behavior. The work presented herein is the first study to develop a methodology to accurately predict local behavior up to and beyond buckling of the PRSEUS stringer. Additionally, the commercially available software, LS-Dyna [17], is used to ensure that the methodology may be readily implemented in industry. One of the primary differences in PRSEUS is the use of stitching to arrest delamination, making it a far more damage tolerant structure than traditional composite structures. However, while this capability has been verified in experiments, conducting these experiments is time-consuming and costly. Accurately simulating the damage development and growth behaviors of PRSEUS parts gives valuable insight into the failure mechanisms and their interactions, allowing the structure to be further optimized. Additionally, these advanced numerical methods would allow PRSEUS to be applied to large-scale structures for dynamic crash analysis or other applications. Eventually, this work may also serve to benefit certification-by-analysis efforts for future airframe development.

## BACKGROUND THEORY

For the damage prediction of composite materials, many failure criteria were developed throughout the mid to late 1900s, such as the Tsai-Wu model in 1970 [18] and Chang-Chang model in 1986 [19], as well as more recent models such as Daimler-Pinho model (2006) [20, 21]. While many theories have been developed, the Tsai-Wu and Chang-Chang composite damage models

are among those that have been commonly implemented into finite element analysis (FEA) software. These damage models do not perfectly represent all of the represented failure mechanisms, but they are widely considered to provide reasonable estimates of the highly non-linear dynamic damage mechanics of composite laminates. For this study, the Chang-Chang model implemented in LS-Dyna was used due to its successful application in prior experience [22,23].

The Chang-Chang composite damage model is an updated form of Hashin's comprehensive composite damage model [24], in which a weight factor ( $\phi$ ) may be added to allow interaction between the shear and fiber tensile failure modes. The model assumes that the unidirectional fiber reinforced composites have a transversely isotropic ( $x_2 = x_3$ ) behavior along the fiber direction ( $x_1$ ). The analytical composite model allows the calculation of stress and damage progression of the fiber and the matrix separately to determine the overall condition of an individual ply. The Chang-Chang failure model of the matrix is described by Eqns. (1) and (2) [19, 24]. The fiber behavior is described by Eqns. (3) and (4) [19, 24].

$$\begin{array}{l} \text{Matrix} \\ \text{Tension:} \end{array} \quad \varepsilon_{mt}^2 = \left(\frac{\sigma_{bb}}{Y_t}\right)^2 + \left(\frac{\sigma_{ab}}{S_c}\right)^2 \quad (1)$$

$$\begin{array}{l} \text{Matrix} \\ \text{Compression:} \end{array} \quad \varepsilon_{mc}^2 = \left(\frac{\sigma_{bb}}{2S_c}\right)^2 + \left[\left(\frac{Y_c}{2S_c}\right)^2 - 1\right] \left(\frac{\sigma_{bb}}{Y_c}\right) + \left(\frac{\sigma_{ab}}{S_c}\right)^2 \quad (2)$$

$$\text{Fiber Tension:} \quad \varepsilon_{ft}^2 = \left(\frac{\sigma_{aa}}{X_t}\right)^2 + \phi \left(\frac{\sigma_{ab}}{S_c}\right)^2 \quad (3)$$

$$\begin{array}{l} \text{Fiber} \\ \text{Compression:} \end{array} \quad \varepsilon_{fc}^2 = \left(\frac{\sigma_{aa}}{X_c}\right)^2 \quad (4)$$

In these equations, subscripts  $m$  and  $f$  are matrix and fiber, respectively, while subscripts  $t$  and  $c$  are the tension and compression, respectively. The fiber direction is  $a$ , while  $b$  and  $c$  are the matrix direction and through-thickness direction, respectively.  $\sigma_{aa}$  is the longitudinal stress of each layer,  $\sigma_{ab}$  is the shear stress of each layer,  $Y$  is the strength of matrix,  $X$  is the strength of fiber, and  $S_c$  is the shear strength in the  $xy$ -plane. Failure occurs when the damage parameter ( $\varepsilon$ ) is equal to or greater than unity.

In addition to the damage that develops within each individual stack, the effects of delamination, interlaminar separation of bonded laminates, must be considered. In the presented computational work, only Mode I and Mode II failures are implemented to predict damage. Mode I fracture is typically a result of through-thickness tensile loading, which can occur between the tear strap and neighboring components for a pressurized vessel. Mode II often occurs during bending, when the outermost plies are subjected to much higher strain than the interior layers. The resulting interlaminar shear stress can cause the epoxy to fail and debonding to occur. For the purposes of the current study, fracture Mode III is assumed to be nearly identical to Mode II separation, with transverse displacement instead of a lateral displacement.

A schematic diagram of the bilinear stress-displacement model that is typically used for mixed-mode cohesive-zone modeling (CZM) is shown in Fig. 3. In this model, critical energy release rate ( $G_c$ ) is the area under a curve defined by peak normal and shear tractions and the crack opening displacement at which the bond has completely failed. The energy release rate of Mode I is defined to be completely independent from the energy release rate of Mode II, but the mixed mode capability combines the energy release rate from each. This capability is necessary because, except for in closely controlled experimental setups, delamination rarely propagates based on a single fracture mode.

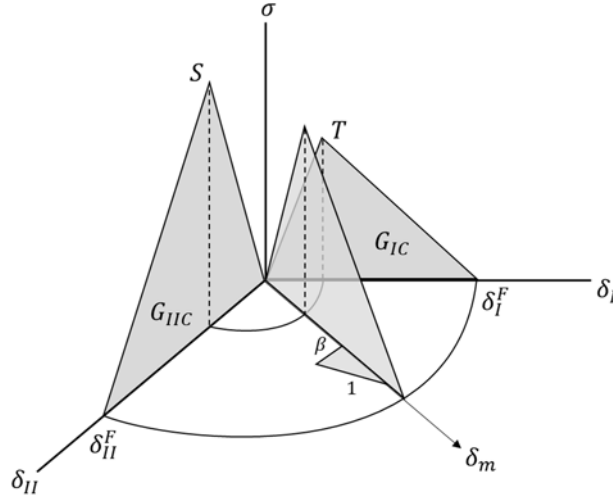


Figure 3. Schematic of the bilinear mixed-mode stress-displacement model

A variant of the traditional bilinear stress-displacement model, the Dycoss Discrete Crack Model [25] is used to approximate the interlaminar bonding. This bilinear model works in both tension and compression, with the initiation of the crack defined using normal ( $\sigma_i$ ) and shear ( $\sigma_{ii}$ ) failure criteria that govern interface strength as shown in Eqn. (5).

$$\left[ \frac{\max(\sigma_i, 0)}{T} \right]^2 + \left[ \frac{\sigma_{ii}}{S - \sin(\theta) \cdot \min(0, T)} \right]^2 = 1 \quad (5)$$

where  $T$  is the allowable normal failure stress and  $S$  is the allowable shear failure stress of interlaminar bonding. An optional friction angle ( $\theta$ ) may be used to approximate woven fabrics, but since unidirectional composites comprise the entirety of PRSEUS, this parameter was negated. Using the tractions of both failure modes allows the model to calculate crack initiation for both single and mixed mode problems. Beyond the initiation of damage, the mixed mode crack propagation is calculated using a power law as shown in Eqn. (6).

$$\left[ \frac{G_I}{G_{IC}} \right]^2 + \left[ \frac{G_{II}}{G_{IIC}} \right]^2 = 1 \quad (6)$$

A distinct energy release rate is assigned for each mode of separation, determined through experimental testing, allowing the delamination to propagate from the initiation zone. This model allows separation to be calculated on a continuous scale from zero to one, where zero represents full adhesion and one represents full separation.

Unlike a traditional cohesive zone model, the Dycoss model does not require an additional layer of elements to be defined at the interface. Instead, a segment based approach is used, in which the element faces of the bonded plies are initially coincident. Because the model does not require a separate material model, the crack opening displacement at failure is approximated based on the penalty contact stiffness. Penalty contact is a method in which artificial springs are placed between a penetrating node and contact interface. By incorporating the interface stiffness directly in the cohesive model, the stability of the simulation is improved.

## MODEL DEVELOPMENT

Multiple PRSEUS stringer configurations have been experimentally tested, but all of the stringer designs have the same baseline architecture. The development and validation of the modeling methodology detailed in the current work is based on the experimental investigation by Leone et al [26], specifically the Class 72 Type 1 stringer without extra adhesive in the overwrap. All of the experimental stringer compression tests were conducted using 0.445-m (17.5-in.) long specimens where 2.54 cm (1 in.) of each end was potted in an epoxy compound within a rectangular steel frame. For each stringer type, only two specimens were tested, so the observed results may not represent the true average response.

The PRSEUS stringer comprises three primary components: the tear strap, pultruded rod, and overwrap. For the current study the tear strap is one stack thick, where the  $0^\circ$  fiber direction is the same as the longitudinal direction of the pultruded rod, which is perpendicular to the primary fiber direction of the skin. The pultruded rod increases the local strength and stability of the stringer while simultaneously increasing the moment of inertia and shifting the neutral axis away from the skin surface. The cross-section of the pultruded rod is actually a teardrop shape to minimize the high matrix concentration deposits near web-rod intersection. The pultruded rod is made from Grafil 34-700WD carbon fibers with PUL6 epoxy resin. All of the stitching is performed using 1600 denier Vectran thread at a spacing of 0.2 stitches per millimeter (5.08 stitches per inch). A schematic of the PRSEUS stringer considered herein is shown in Fig. 4.

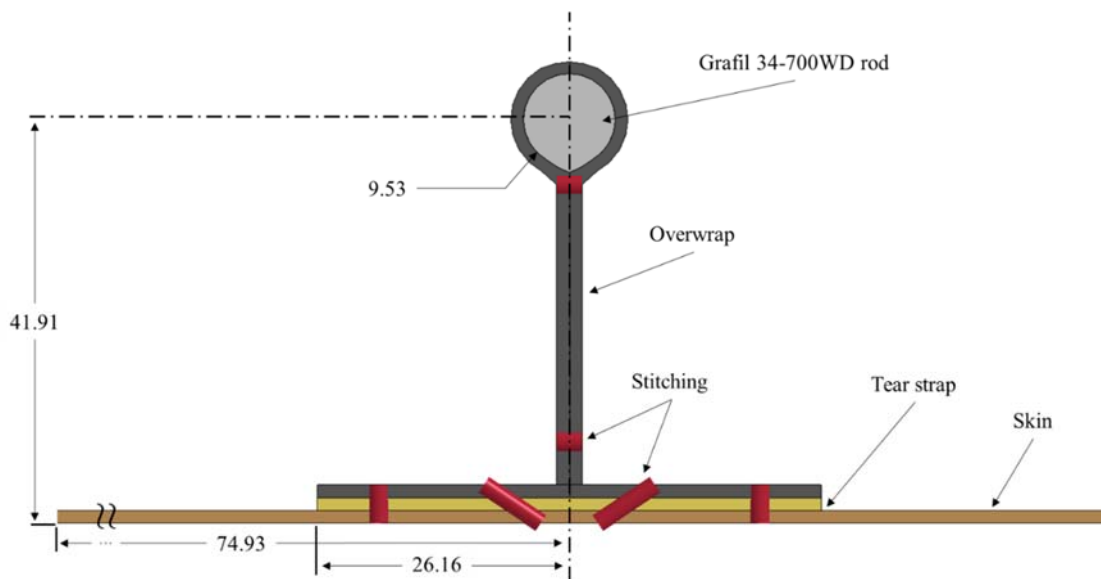


Figure 4. Schematic of the PRSEUS stringer in the current analysis (all dimensions are in mm)

Several configurations of a PRSEUS stringer were previously considered. In this study, a single configuration is considered, and all discussions pertain to only this configuration. The pultruded rod is attached to the stringer by an overwrap stack that is stitched to the tear strap. The overwrap is a single continuous stack, producing a web that is two stacks thick. PRSEUS utilizes a unique stitching structure to bind the stringer elements together, with six stitch paths in total. One stitch path is applied through the top of the web to fix the rod location while a second stitch path is applied just above the point where the web stack is folded out to become the flange. The final stitch paths are located in the flange; a 45° stitch sewed through the overwrap, tear strap, and skin toward the stringer centerline near the web. Possibly the most critical stitch location is at the overwrap and tear strap edge, since this stitch row prevents any initial delamination within the skin or between the skin and tear strap from propagating toward the stringer center [27].

Two fundamentally different computational models were created for the analysis of the stringer, as shown in Fig. 5. The first model utilized a tiebreak approach to simulate both the stitching and epoxy. Although computationally expensive, tiebreak models are commonly used to represent stitch bonding [28]. However, this approach is highly mesh-dependent and can only approximate some aspects of the unique stitching configuration required for PRSEUS (i.e., the 45° stitches through the web, tear strap, and skin). Additionally, while the tiebreak approach allows stress concentrations to form at the stitch interface between layers, that approach ignores the through-thickness stress concentrations that would be present in the actual specimen.

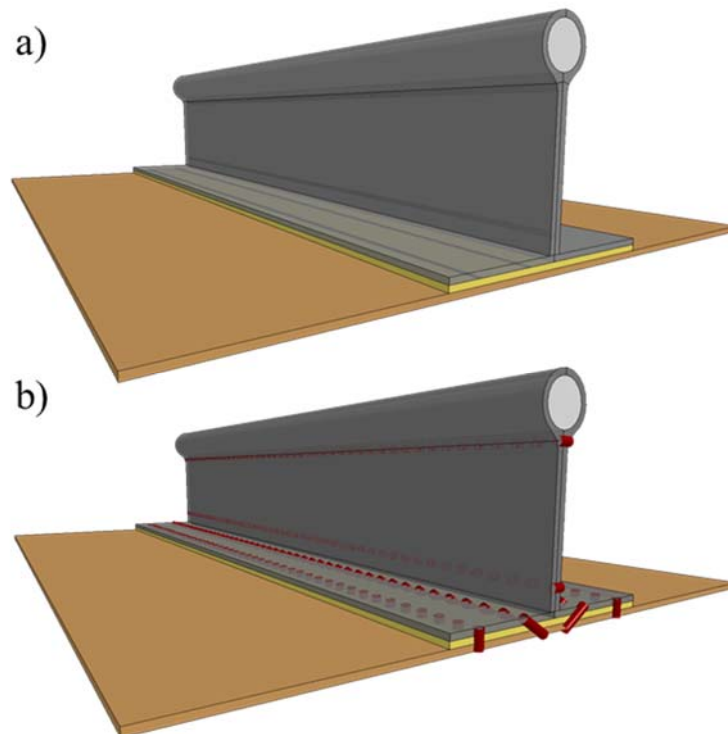


Figure 5. PRSEUS stringer model using tiebreak (top) and beams (bottom) for stitching

Therefore, a second and arguably higher fidelity approach was created that individually models each through-thickness stitch. Instead of modeling each stitch as an actual penetration in the stack, the nodes on either side of the stitch location are connected with a beam element.

Modeling each stitch as a beam allows the through-thickness tensioning effect to be captured under deformation. Since there is no direct connection to the interlaminar surface, the beam approach relies on the local stress concentration and friction to simulate the effect of the embedded stitch. For both of these modeling strategies, the location of the nodes is of critical importance to accurately represent the placement of the stitching. Another strength of the beam stitching approach is that this approach is theoretically less mesh dependent as long as the maximum element size is no greater than the minimum distance between each stitch.

Considering the necessity of computational efficiency in simulation-aided design and optimization, several strategies were implemented to minimize computation time while maintaining high accuracy. A symmetric boundary condition is used at the mid-surface of the PRSEUS stringer to reduce computational time. Selectively reduced integration with solid elements were used to represent all of the stack material in the model. No under-integrated elements were used because initial tests showed that hourglass energy could not be effectively mitigated with the available hourglass energy controls. An extremely important aspect of the model is the definition of the local material angle throughout the stringer, as illustrated in Fig. 6. If the material angle did not correspond to changes in curvature, then the response of the structure would be severely affected. Due to a limitation in the software that prevented the correct use of tiebreak contact with implicit analysis, all simulations were performed using explicit analysis. Considering the quasi-static loading of the experimental testing, a preliminary parametric study was performed to determine that an accelerated loading rate of 0.125 m/s (0.41 ft/s) could be used without significantly affecting the structural response.

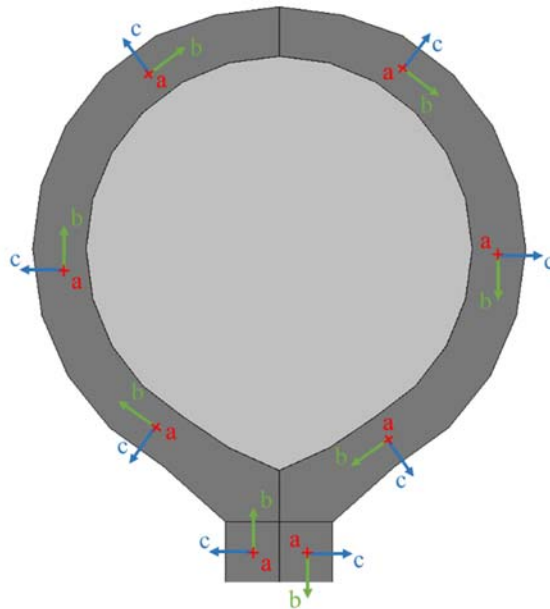


Figure 6. Illustration of local material angle along the overwrap for the pultruded rod

The interfaces between stacks are defined using the previously discussed Dycoss Discrete Crack model. The Mode I separation properties at the interface are typically found through a double cantilever beam (DCB) test, which was conducted by Grenoble et al. for  $[0/90]_s$  preforms of the Class 72 material [29]. While the study provides a the Mode I energy release rate of 390.53



$J/m^2$  (2229.2 lb-f/in<sup>2</sup>) the report does not provide either peak traction or maximum crack opening displacement when full debonding occurs. Therefore, an iterative approach is used in which an initial estimate of the peak normal traction is made and then the corresponding load versus opening displacement curve is plotted. This process is repeated until a reasonable agreement is achieved between the experimental and computational predictions. Because the results of the analysis depend on both the grid refinement [30, 31] and the peak traction selected [32], the analysis was conducted using a mesh refinement that had been selected based on the geometry and scale of the stringer. The numerical results from three peak traction estimates are plotted and compared in Fig. 7 to the experimental load-displacement measurements. The 30 MPa (4.35 ksi) peak normal traction has the best fit, due to its correlation with the peak load and stability. The higher peak tractions were discounted because the debonding at each node resulted in an unstable crack growth for the chosen level of mesh refinement.

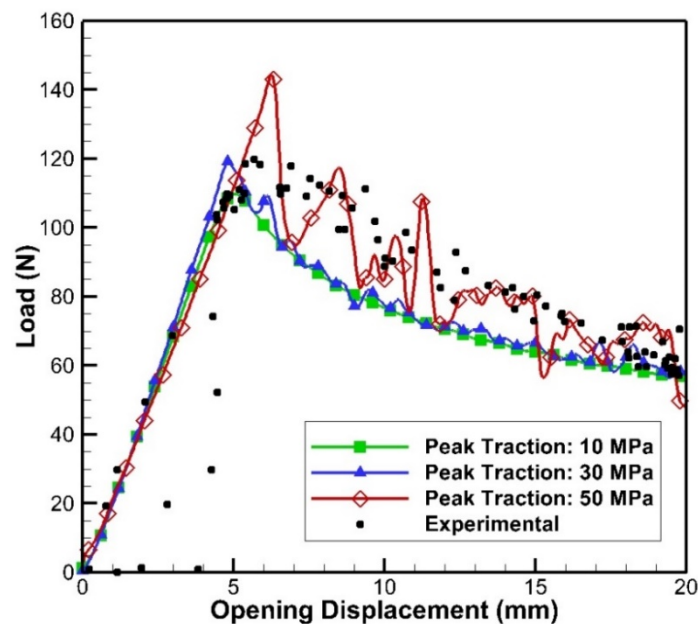


Figure 7. Load versus opening displacement for each simulated peak traction (all experimental cases are plotted)

The presence of the epoxy potting used in the experiment is also an important consideration that can significantly affect the effective stiffness of the stringer. As illustrated in Fig. 8, three different boundary conditions were investigated to accurately reproduce the effect of the epoxy. The highest fidelity approach directly models the surrounding epoxy and requires significantly more elements, whereas the lowest fidelity approach does not include the potted material and applies a fully fixed condition. The low-fidelity model has a significant advantage in computational time because the length of the stringer is reduced by the width of the potting. Between these two extremes is the pseudo-epoxy boundary which restricts transverse translation, but allows the potted material to compress in the loading direction. A preliminary study found that this boundary was capable of predicting the effective stiffness with only 0.1% error at a significantly lower computational cost. Alternatively, the low-fidelity boundary resulted in a structural response that over-predicted the stiffness by 15%.

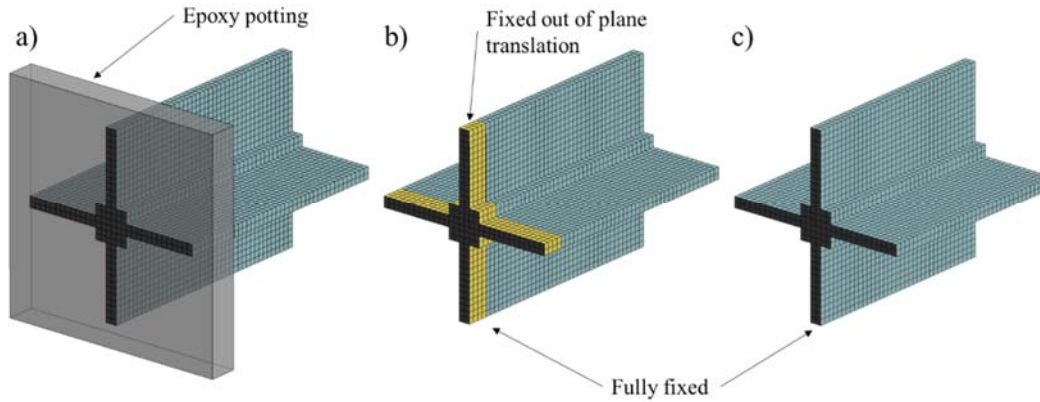


Figure 8. Illustration of the three tested boundary conditions: a) high fidelity, b) pseudo-epoxy, c) low fidelity

The final model consists of 35,910 solid elements, 276 beam elements, and 68,818 nodes. The large disparity between the number of elements and nodes is a result of including the capability to represent delamination between stack layers. Finally, static and dynamic coefficients of friction for stack interaction were defined to be 0.65 and 0.40, respectively, based on existing literature [33, 34]. The development of the computational setup and input parameters is discussed in [35].

## RESULTS AND VALIDATION

The load-displacement relationship for each modeling approach, the experimental baseline, and the numerical results by Leone et al, are shown in Fig. 9. The initial material inputs used for the analysis are a result of averaging the tension and compression stack properties reported for PRSEUS [12] and are listed in Table 1. Initial properties for the pultruded rod are also taken from [12], in which Toray T800 fibers were used with a 3900-2B resin.

Table 1. Summary of updated material properties based on stiffness knockdown factors

Part	Property	Initial Input	Updated Input
Class 72 Type 1 Stack	$E_x$ (GPa)	67.2	65.0
	$E_y$ (GPa)	33.6	32.0
	$G_{xy}$ (GPa)	16.4	15.6
	$\nu_{xy}$	0.400	0.400
Pultruded Rod	$E_x$ (GPa)	137.0	109.6

Compared to the experimental baseline, both of the predicted curves from the current study are overly stiff, though they are less stiff than the results calculated by Leone et al. Despite the increased stiffness, both the tiebreak and beam-stitch approaches correlate well with the buckling load from the experiment, each with less than 1% error in peak magnitude. Alternatively, only a change in stiffness is observed for the existing numerical model, with no reduction in the load that would indicate buckling. The post-buckling response of both the tiebreak-stitch and beam-stitch models approximately match the trends from the experiment, though both display much greater oscillation in the post-buckling load than was observed for the test specimens. The displacement

oscillations could be a result of the loading rate required to effectively conduct the explicit analysis, though this hypothesis cannot be confirmed without incurring extreme computation time. In general, the two models performed similarly, achieving the same exact stiffness up until buckling and then both peaking at approximately 142 kN (319 kips). Additionally, the computational effort required by each approach was nearly the same. The beam-stitch model reached simulation termination slightly faster than the tiebreak-stitch model, but this slight difference may be a result of the extra contact algorithm required for the tiebreak stitches or due to interference from other computational processes.

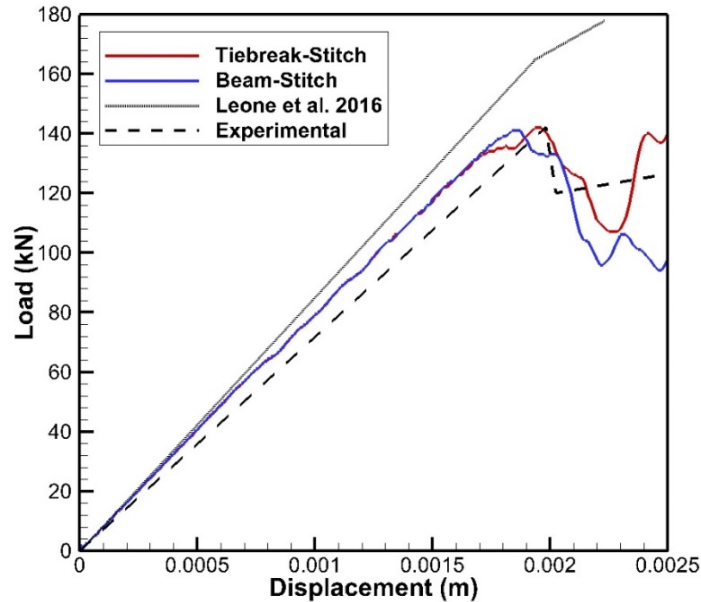


Figure 9. Load versus displacement for both the tiebreak-stitch and beam-stitch stringer models

Although the results of the models are comparable, the beam-stitch approach could be more easily implemented, since the tiebreak-stitch approach requires additional manual effort by the user, slowing the overall process. Therefore, the beam-stitch approach was selected for further application. Additionally, the lower mesh dependency of the beam-stitch approach makes it a more feasible option at large scales.

The high stiffness predicted by both the tiebreak-stitch and beam-stitch models is an unexpected response that prompts a more thorough investigation of the material property inputs. Upon further investigation, the material parameters for both the Class 72 stack material and Grafil 34-700WD rod were updated. An experimental investigation of stitched versus un-stitched material by Grenoble and Johnston [29] indicates that the stitched material incurs a loss in both axial moduli and strength as a result of the fiber misalignment and imperfections introduced by the stitch. Although the difference is only compared for specimens loaded in tension, it is expected that a similar trend would be observed in compression and transverse directions. Based on the results of the study, both the axial and lateral stiffness inputs are reduced by approximately 5%, which is reflected in Table 1. No significant difference in Poisson's ratio is observed between the two configurations.

Unlike the pultruded rod properties used for the initial material definition, the pultruded rod used in the current study is composed of Grafil 34-700 fibers and PUL6 epoxy. No information about PUL6 or the fiber volume fraction of the pultruded rod was found in the public domain, so the properties of the pultruded rod were scaled based on the previous candidate material for the stringer rod. The parameters reported in the Grafil 34-700 fiber datasheet [36] are based on a 60% fiber volume fraction combination of Grafil 34-700 fibers and Mitsubishi Rayon #340 resin instead of the PUL6 epoxy used in the PRSEUS stringer. By comparing the relative reduction in fiber stiffness between the pultruded rod properties from [12] with the properties reported in the Toray datasheet [37], a scale factor was calculated for the rod moduli. The scale factor was then applied to the Grafil 34-700 datasheet properties to approximate the correct pultruded rod stiffness. The resulting material input for the pultruded rod is listed in Table 1.

With the updated material parameters, the PRSEUS stringer is simulated at the progressive stages of model development shown in Fig. 10. Initially, just the stringer model with no interlaminar bonding or stitching is simulated, providing resistance from geometric effects alone. As expected, the overwrap flange detaches from the tear strap and the web stacks separate from one another early in the loading history, losing structural integrity. After separation of the individual components, the majority of the load is supported by the pultruded rod until it buckles. When the effect of the epoxy is added to the model, a significant gain in strength is observed, increasing the buckling load to three times the no-epoxy result. The interlaminar bonding does not appreciably affect the stiffness of the specimen, matching the stiffness of the un-bonded model until 0.8 mm (0.031 in.) of applied displacement. Beyond this point, the deviation in effective stiffness between the prediction and experimental test increases to 7.3%, compared to the initial slope error of 0.8%. Once buckling occurs, the load-bearing capacity of the structure quickly drops to near zero, which is characteristic of typical composites.

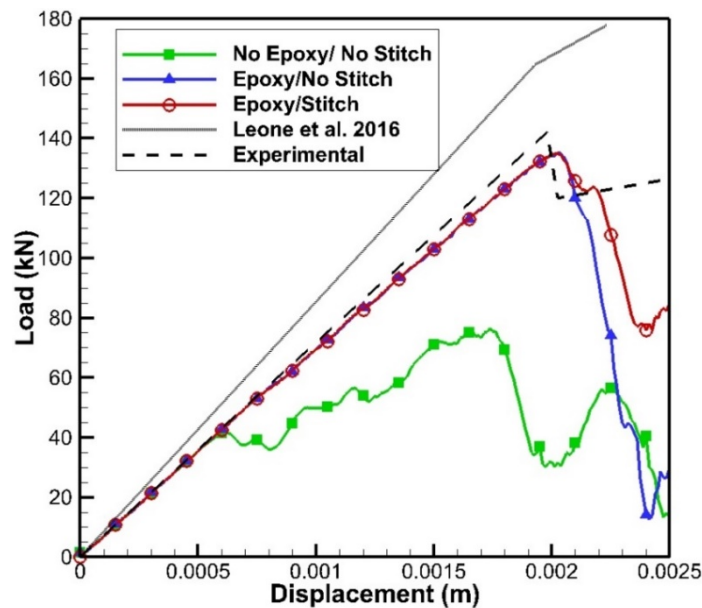


Figure 10. Loading versus displacement response for progressive development of the PRSEUS stringer with updated material properties

The final model with both stitching and epoxy indicates that stitching primarily improves the post-buckling response of the structure. No significant increase in peak load is observed, but including the stitching allows the structure to support load after the initial buckling. While the magnitude of the post-buckled load being supported is under-predicted by the simulation, it follows the same trend as observed in the experiment.

## CONCLUSIONS

A steep increase in demand for fuel-efficient aviation as a result of environmentally responsible initiatives and elevated fuel costs has prompted a revolution in modern aircraft. The HWB concept promises improved energy and space efficiency compared to current aircraft, but requires new technologies to be developed to support the loads introduced by the HWB unique geometry. By introducing a unique damage-tolerant construction, PRSEUS is capable of withstanding the complex loading expected in the HWB. However, while many proof-of-concept tests have been performed, accurate and high-fidelity computational tools are required to develop PRSEUS further without excessive experimental cost. Such tools will also be necessary for commercial certification and implementation.

The work described herein addresses the necessity of commercial certification and implementation by demonstrating a comprehensive modeling approach that investigates PRSEUS with a higher fidelity as compared to existing computational analyses. The majority of available experiments for comparison have been conducted at the coupon level. Therefore, a computational methodology was progressively developed, based on physically realistic concepts, with minimal use of computational tuning parameters. A high-fidelity stringer model was created at the coupon scale and thoroughly developed with a series of investigations to determine the necessary approach to consistently achieve accurate results. Both tiebreaks and beam elements were considered to model the stitching, though the beam-stitch approach was selected due to its relatively simple implementation and better representation of the PRSEUS concept. Important parameters including local material direction, bonding strength between stacks, and boundary conditions are clearly identified. The model was analyzed at several stages of development to demonstrate the individual effect of epoxy bonding and stitching.

The final methodology was successfully validated against an experimental baseline and was capable of achieving significantly greater accuracy than models currently in the literature. Despite slight deviations in the slope and post-buckling response, as a result of the fast loading rate, the final stringer model with interlaminar bonding and stitching provided highly accurate predictions. The error in effective stiffness is initially less than 1% while the predicted peak buckling load deviates less than 4% between computational results and experimental data. Additionally, the developed methodology extends the capability of the prediction to include a post-buckling response. With the predictive capabilities and unique insight provided, the work herein may serve to benefit future iterations of PRSEUS and other structures with through-thickness reinforcement.

## ACKNOWLEDGEMENTS

The award of a grant under “Multiscale Modeling of Advanced Aerospace PRSEUS Structures” by the NASA Environmentally Responsible Aviation (ERA) Program and National Institute for Aerospace (NIA) is highly acknowledged. Additionally, the input of Dr. Frank Leone is greatly appreciated.

## REFERENCES

- [1] Jegley D, Velicki A. Status of Advanced Stitched Unitized Composite Aircraft Structures. 51st AIAA Aerosp. Sci. Meet. Incl. New Horizons Forum Aerosp. Expo., Grapevine, Texas: 2013, p. 1–12. doi:10.2514/6.2013-410.
- [2] Okonkwo P, Smith H. Review of Evolving Trends in Blended Wing Body Aircraft Design. *Prog Aerosp Sci* 2016;82:1–23. doi:10.1016/J.PAEROSCI.2015.12.002.
- [3] Liebeck RH. Design of the Blended Wing Body Subsonic Transport. *J Aircr* 2004;41:10–25. doi:10.2514/1.9084.
- [4] Reist TA, Zingg DW. High-Fidelity Aerodynamic Shape Optimization of a Lifting-Fuselage Concept for Regional Aircraft. *J Aircr* 2017;54:1085–97. doi:10.2514/1.C033798.
- [5] Nickol C, Mccullers L. Hybrid Wing Body Configuration System Studies. 47th AIAA Aerosp. Sci. Meet. Incl. New Horizons Forum Aerosp. Expo., Orlando, Florida: 2009, p. 1–12. doi:10.2514/6.2009-931.
- [6] Lyu Z, Martins JRRA. Aerodynamic Design Optimization Studies of a Blended-Wing-Body Aircraft. *J Aircr* 2014;51:1604–17. doi:10.2514/1.C032491.
- [7] Dae Kim H, L. Felder J, T. Tong M, J. Berton J, J. Haller W. Turboelectric Distributed Propulsion Benefits on the N3-X Vehicle. *Aircr Eng Aerosp Technol* 2014;86:558–61. doi:10.1108/AEAT-04-2014-0037.
- [8] Czech MJ, Thomas RH, Elkoby R. Propulsion Airframe Aeroacoustic Integration Effects for a Hybrid Wing Body Aircraft Configuration. *Int J Aeroacoustics* 2012;11:335–68. doi:10.1260/1475-472X.11.3-4.335.
- [9] Lovejoy AE. Optimization of Blended Wing Body Composite Panels Using Both NASTRAN and Genetic Algorithm. NASA/CR-2006-214515. Hampton, VA: 2006.
- [10] Lovejoy AE. PRSEUS Pressure Cube Test Data and Response. NASA/TM–2013-217795. Hampton, VA: 2013.
- [11] Niggemann C, Young Seok Song YS, Gillespie JW, Heider D. Experimental Investigation of the Controlled Atmospheric Pressure Resin Infusion (CAPRI) Process. *J Compos Mater* 2008;42:1049–61. doi:10.1177/0021998308090650.
- [12] Velicki A. Damage Arresting Composites for Shaped Vehicles - Phase I Final Report. NASA/CR-2009-215932. Hampton, VA: 2009.
- [13] Velicki A, Thrash P, Jegley D. Airframe Development for the Hybrid Wing Body Aircraft. 47th AIAA Aerosp. Sci. Meet. Incl. New Horizons Forum Aerosp. Expo., Orlando, Florida: 2009, p. 1–8. doi:10.2514/6.2009-932.
- [14] Yovanof N, Jegley D. Compressive Behavior of Frame-Stiffened Composite Panels. 52nd AIAA/ASME/ASCE/AHS/ASC Struct. Struct. Dyn. Mater. Conf., Denver, Colorado: 2011, p. 1–

15. doi:10.2514/6.2011-1913.
- [15] Bergan A, Bakuckas J, Awerbuch J, Tan T-M. Assessment of Damage Containment Features of a Full-scale PRSEUS Fuselage Panel. *Compos Struct* 2014;113:174–85. doi:10.1016/j.compstruct.2014.03.011.
- [16] Lovejoy AE, Rouse M, Linton KA, Li VP. Pressure Testing of a Minimum Gauge PRSEUS Panel. 52nd AIAA/ASME/ASCE/AHS/ASC Struct. Struct. Dyn. Mater. Conf., Denver, Colorado: 2011, p. 1–18. doi:10.2514/6.2011-1813.
- [17] Hallquist JO. LS-DYNA Theory Manual. Livermore, CA: 2015.
- [18] Tsai SW, Wu EM. A General Theory of Strength for Anisotropic Materials. *J Compos Mater* 1971;5:58–80. doi:10.1177/002199837100500106.
- [19] Chang F-K, Chang K-Y. A Progressive Damage Model for Laminated Composites Containing Stress Concentrations. *J Compos Mater* 1987;21:834–55. doi:10.1177/002199838702100904.
- [20] Pinho ST, Iannucci L, Robinson P. Physically-based Failure Models and Criteria for Laminated Fibre-reinforced Composites with Emphasis on Fibre Kinking. Part I: Development. *Compos Part A Appl Sci Manuf* 2006;37:63–73. doi:10.1016/j.compositesa.2005.04.016.
- [21] Pinho ST, Iannucci L, Robinson P. Physically-based Failure Models and Criteria for Laminated Fibre-reinforced Composites with Emphasis on Fibre Kinking. Part II: FE Implementation. *Compos Part A Appl Sci Manuf* 2006;37:766–77. doi:10.1016/j.compositesa.2005.06.008.
- [22] Schroeder K, Song Y, Horton B, Bayandor J. Investigation of UAS Ingestion into High-Bypass Engines, Part 2: Parametric Drone Study. 58th AIAA/ASCE/AHS/ASC Struct. Struct. Dyn. Mater. Conf., Grapevine, Texas: 2017. doi:10.2514/6.2017-0187.
- [23] Song Y, Bayandor J. Analysis of Progressive Dynamic Damage Caused by Large Hailstone Ingestion into Modern High Bypass Turbofan Engine. 57th AIAA/ASCE/AHS/ASC Struct. Struct. Dyn. Mater. Conf., San Diego, California: 2016, p. 1–14.
- [24] Hashin Z. Failure Criteria for Unidirectional Fiber Composites. *J Appl Mech* 1980;47:329–34. doi:10.1115/1.3153664.
- [25] Lemmen P, Meijer G-J, Rasmussen EA. Dynamic Behaviour of Composite Ship Structures (DYCOSS) - Failure Prediction Tool. 70th Shock Vib. Symp., Albuquerque, NM: 1999.
- [26] Leone FA. Pultruded Rod / Overwrap Testing for Various Stitched Stringer Configurations. NASA/TM-2016-218975. Hampton, VA: 2016.
- [27] Velicki A, Thrash P. Damage Arrest Design Approach using Stitched Composites. *Aeronaut J* 2011;115:789–95. doi:10.1017/S0001924000006539.
- [28] Bergan AC. Test and Analysis of Stitched Composite Structures to Assess Damage Containment Capability. Drexel University, 2014. doi:10.1017/CBO9781107415324.004.
- [29] Grenoble RW, Johnston WM. Material Property Characterization of AS4/VRM-34 Textile Laminates. NASA/TM-2013-218050. Hampton, VA: 2013.
- [30] Arablouei A, Kodur V. Modeling Delamination of Fire Insulation from Steel Structures Subjected to Blast Loading. *Eng Struct* 2016;116:56–69. doi:10.1016/j.engstruct.2016.02.042.
- [31] Ericsson M. Simulating Bird Strike on Aircraft Composite Wing Leading Edge. KTH Royal Institute of Technology, 2012.

- [32] LS-DYNA Aerospace Working Group Modeling Guidelines Document. 2014.
- [33] Schön J. Coefficient of Friction and Wear of a Carbon Fiber Epoxy Matrix Composite. *Wear* 2004;257:395–407. doi:10.1016/j.wear.2004.01.008.
- [34] Roselman IC, Tabor D. The Friction of Carbon Fibres. *J Phys D Appl Phys* 1976;9:2517–32. doi:10.1088/0022-3727/9/17/012.
- [35] Horton B. Comprehensive Multi-Scale Progressive Failure Analysis for Damage Arresting Advanced Aerospace Hybrid Structures. Virginia Tech, 2017.
- [36] Grafil Inc. Grafil 34-700. Sacramento: n.d.
- [37] Toray Carbon Fibers America I. Torayca Data Sheet. Santa Ana: n.d.